Atmospheric Environment 59 (2012) 559–566

Contents lists available at SciVerse ScienceDirect

Atmospheric Environment

journal homepage: www.elsevier.com/locate/atmosenv

Impacts of aerosol compositions on visibility impairment in Xi'an, China

Jun-ji Cao [a,c,*], Qi-yuan Wang [b], Judith C. Chow [a,d], John G. Watson [a,d], Xue-xi Tie [a,e], Zhen-xing Shen [b], Ping Wang [a], Zhi-sheng An [a]

[a] Key Laboratory of Aerosol, SKLLQG, Institute of Earth Environment, Chinese Academy of Sciences, Xi'an 710075, China
[b] Department of Environmental Science and Engineering, Xi'an Jiaotong University, Xi'an 710049, China
[c] Institute of Global Environmental Change, Xi'an Jiaotong University, Xi'an 710049, China
[d] Desert Research Institute, Reno, NV, USA
[e] National Center for Atmospheric Research, Boulder, CO, USA

HIGHLIGHTS

- Visibility was an average visual range of 6.4 km at Xi'an.
- $PM_{2.5}$ concentration, corresponding to the low visibility (<10 km), was ~88 μg m^{-3}.
- $PM_{2.5}$ ammonium sulfate accounted for ~40% of light extinction.

ARTICLE INFO

Article history:
Received 24 November 2011
Received in revised form
16 May 2012
Accepted 17 May 2012

Keywords:
Visibility impairment
Light extinction coefficient
Chemical species
Source apportionment

ABSTRACT

Daily particle light scattering coefficient, $PM_{2.5}$ mass and chemical composition were measured in Xi'an from February to December 2009. Visibility was strongly affected by anthropogenic air pollution sources, resulting in an average visual range (VR) of 6.4 ± 4.5 km. The threshold $PM_{2.5}$ mass concentration, corresponding to VR <10 km, was ~88 μg m^{-3}. The revised IMPROVE equation was applied to estimate chemical extinction (b_{ext}), which on average was ~15% lower than measured b_{ext}. $PM_{2.5}$ ammonium sulfate was the largest contributor, accounting for ~40% of b_{ext}, followed by organic matter (~24%), ammonium nitrate (~23%), and elemental carbon (~9%), with minor contributions from soil dust (~3%), and NO_2 (~1%). High secondary inorganic aerosol contributions (i.e., SO_4^{2-} and NO_3^-) were the main contributors for VR <5 km. A Positive Matrix Factorization (PMF) solution to the Chemical Mass Balance (CMB) receptor model showed that coal combustion was the dominant factor, accounting for ~52% of the dry particle light scattering coefficient, followed by the engine exhaust factor (~31%). Other factors included biomass burning (~12%) and fugitive dust (~5%).

1. Introduction

Visibility is an indicator of urban air quality. Urban and regional visibility has been deteriorating in China in concert with economic growth and increasing emissions (Chang et al., 2009; Che et al., 2009). Intense "haze-fog" events in Beijing during late October of 2011 (e.g., http://news.yzdsb.com.cn/system/2011/11/10/011485620_01.shtml) raised public awareness of adverse effects associated with visibility impairment.

Xi'an, one of the largest cities in China, is situated on the Guanzhong Plain at the southern edge of the Loess Plateau with a resident population of eight million and two million visitors per year. Twenty-four hour average $PM_{2.5}$, which scatters and absorbs light (Chow et al., 2002a; Watson, 2002), ranged from 130 to 351 μg m^{-3} in Xi'an (Cao et al., 2005; Han et al., 2010; Shen et al., 2009), exceeding the Chinese government's recently issued 24-h $PM_{2.5}$ standard of 75 μg m^{-3} by two- to five-fold (http://www.chinadaily.com.cn/china/2012-03/03/content_14745568.htm). From 1995 to 2005, visual range (VR; the farthest distance at which the human eye can distinguish a target against a background; Booker and Douglas, 1977) decreased ~5.71 km, with a VR of 5.13 km in 2007 (Chang et al., 2009). Days with low visibility (i.e., VR <10 km) increased by ~sevenfold from 50 days in 1995 to 340 days in 2007.

In 2003, the "Blue Sky Project" for visual air quality improvement was initiated to investigate the extent of pollution control measures needed in Xi'an. The Shaanxi provincial government has

* Corresponding author. Key Laboratory of Aerosol, SKLLQG, Institute of Earth Environment, Chinese Academy of Sciences, Xi'an 710075, China. Tel.: +86 29 8832 6488; fax: +86 29 8832 0456.
E-mail address: cao@loess.llqg.ac.cn (J.-j. Cao).

1352-2310/$ – see front matter © 2012 Elsevier Ltd. All rights reserved.
http://dx.doi.org/10.1016/j.atmosenv.2012.05.036

taken actions to reduce emissions such as: installing and operating sulfur dioxide (SO_2) scrubbers on coal-fired power stations, using cleaner coals for large-scale boilers, substituting coal with cleaner fuels (e.g., liquefied petroleum gas, LPG) for domestic cooking and heating, and modernizing the urban vehicle fleet. These measures, however, have not improved air quality as anticipated. A good understanding of the causes of poor visibility is needed to implement effective emission reduction strategies. Improvements in visibility will also have co-benefits for public health, material and crop damage, and climate (Chow and Watson, 2011).

The objectives of this study are to: (1) examine the seasonal variations of VR and light extinction (b_{ext}); and (2) assess the causes of visibility impairment by relating b_{ext} to $PM_{2.5}$ chemical composition.

2. Sampling and analysis

Sampling was conducted from February 15 to December 31, 2009, at an urban-scale (Chow et al., 2002b) site on the rooftop (~10 m above ground level) of the Institute of Earth Environment, Chinese Academy of Sciences (IEECAS; Cao et al., 2009). This site is located ~15 km southwest of downtown Xi'an in a residential/commercial neighborhood.

Twenty-four hour $PM_{2.5}$ samples were collected daily from 1000 local standard time (LST) to 1000 LST the next day using a battery-powered mini-volume sampler (Airmetrics, Oregon, USA) with a flow rate of 5 L min^{-1}. Quartz-fiber filters of 47 mm diameter (QM/A; Whatman, Middlesex, UK) were used for mass, elements, water-soluble ions, and organic and elemental carbon (OC and EC, respectively) analyses. The quartz-fiber filters were preheated to 800 °C for 3 h before sampling and equilibrated using controlled temperature (20–23 °C) and relative humidity (RH; 35–45%) desiccators before and after sampling for 24 h prior to weighing on a Sartorius MC5 electronic microbalance with a ±1 μg sensitivity (Sartorius, GÖttingen, Germany). Samples were stored air-tight in a refrigerator at about 4 °C before chemical analysis to prevent evaporation of volatilized components.

The elemental concentrations were determined by Energy Dispersive X-Ray Fluorescence (ED-XRF) spectrometry (Epsilon 5 ED-XRF, PANalytical B.V., the Netherlands). The Epsilon 5 spectrometer uses a three-dimensional polarizing geometry with 11 secondary targets (i.e., CeO_2, CsI, Ag, Mo, Zr, KBr, Ge, Zn, Fe, Ti, and Al) and one barkla target (Al_2O_3) that supplies a good signal–background ratio, and provides low detection limits (Watson et al., 1999). The X-ray source is a side window X-ray tube with a Gadolinium (Gd) anode, operated at an accelerating voltage of 25–100 kV and a current of 0.5–24 mA (maximum power: 600 W). The X-ray characteristic radiation is detected by a Germanium (Ge) detector (PAN 32). Each sample was analyzed for 30 min and laboratory quartz-fiber filter blanks were analyzed to evaluate analytical bias. The 10 elements determined by the ED-XRF method were Ca, Mg, S, K, Ti, Mn, Fe, As, Br, and Pb.

Water-soluble ions were determined by ion chromatography (Chow and Watson, 1999) (IC, Dionex 600, Dionex Corp, Sunnyvale, CA). Cations, including Mg^{2+}, K^+, Ca^{2+}, and NH_4^+, were determined using a CS12A column (Dionex Company) with 20 mM methanesulfonic acid eluent. Anions, including F^-, Cl^-, NO_3^-, and SO_4^{2-} were determined using an ASII-HC column (Dionex Company), with 20 mM potassium hydroxide (KOH) eluent. The detection limits were less than 0.05 mg L^{-1} for cations and anions. Standard Reference Materials produced by the National Research Center for Certified Reference Materials in China were analyzed for quality assurance (QA)/quality control (QC) purposes.

Carbonaceous species (OC, EC and carbon fractions) were analyzed using the thermal/optical reflectance (TOR) method (Chow et al., 1993, 2001, 2004, 2005, 2007, 2011) on a DRI Model 2001 Thermal/Optical Carbon Analyzer (Atmoslytic Inc., Calabasas, CA, USA). The IMPROVE_A protocol (Chow et al., 2007) produces four OC fractions (OC1, OC2, OC3, and OC4 in a 100% helium (He) atmosphere at 140 °C, 280 °C, 480 °C, and 580 °C, respectively); a pyrolyzed carbon fraction (OP, determined when reflected laser light attained its original intensity after oxygen (O_2) was added to the analysis atmosphere); and three EC fractions (EC1, EC2, and EC3 in a 98% He/2% O_2 atmosphere at 580 °C, 740 °C, and 840 °C, respectively). OC is defined as OC1 + OC2 + OC3 + OC4 + OP and EC as EC1 + EC2 + EC3 − OP. The analyzer was calibrated daily with known quantities of methane (CH_4) (Chow et al., 2011).

Replicate analyses were performed on 10% of the samples. Average field blanks were subtracted and their associated uncertainties propagated to correct for passive deposition, especially the positive organic artifact due to adsorption of gas-phase organic components onto the filter during and/or after sampling (Chow et al., 2010a; Watson et al., 2009). More detailed descriptions of QA/QC procedures can be found in Cao et al. (2003) and Chow et al. (2011).

Five-minute averaged dry particle light scattering coefficient ($b_{scat,dry}$) was measured by Aurora-1000 single wavelength (λ = 520 nm) integrating nephelometer equipped with a smart heater (Ecotech, Melbourne, Australia). Span calibration was carried out every month using R-134 gas, while zero calibration was performed every two days with particle-free air to subtract the Rayleigh scattering. The nephelometer draws the ambient air through a heated inlet at a flow rate of 5 L min^{-1} to retain RH <60%.

Five-minute averaged nitrogen dioxide (NO_2) gas was measured gas-phase chemiluminescence (Ecotech EC9841 Nitrogen Oxides Analyzer), with lower quantifiable limits of 0.5 ppb. Hourly wind speed (WS), temperature, RH, and atmospheric pressure were obtained from the Xi'an Meteorological Bureau, ~25 km north from the sampling site. Wind direction data was not available.

3. Data analysis

The light extinction coefficient, b_{ext}, is defined as the sum of the $PM_{2.5}$ scattering (b_{sp}), $PM_{2.5}$ absorption (b_{ap}), gas (NO_2) absorption (b_{ag}), and Rayleigh scattering (b_{sg}) (Watson, 2002), where:

$$b_{ext} = b_{sp} + b_{ap} + b_{ag} + b_{sg} \quad (1)$$

b_{ext} values can approximate VR using the Koschmieder (1924a,b) equation:

$$VR = 3.912/b_{ext} \quad (2)$$

Hygroscopic particles such as sulfates and nitrates grow into more efficient light-scattering sizes with increasing RH (Chow et al., 2002a). According to relationships described by Pitchford et al. (2007), this growth is approximated by:

$$b_{sp,wet} = f(RH) \times b_{sp,dry} \quad (3)$$

where $b_{sp,wet}$ is the wet scattering coefficient, f(RH) is the growth function, and $b_{sp,dry}$ is the dry scattering coefficient measured by nephelometer at RH < 60%. The f(RH) curve from Malm et al. (2003) was used for this study.

The absorption coefficient, b_{ap}, is approximated by applying the IMPROVE mass extinction efficiency of 10 m^2 g^{-1} to the EC concentration (Chow et al., 2010b; Pitchford et al., 2007; Watson, 2002):

$$b_{ap}\left(Mm^{-1}\right) = 10\left(m^2\ g^{-1}\right) \times [EC]\left(\mu g\ m^{-3}\right) \quad (4)$$

Gaseous NO_2 absorption is estimated by using the absorption efficiency of Hodkinson (1966):

$$b_{ag}\left(Mm^{-1}\right) = 0.33 \times [NO_2](ppb). \quad (5)$$

The Rayleigh scattering coefficient (b_{sg}) was assumed to be a constant value of 10 Mm^{-1} at sea level (Watson, 2002).

The revised IMPROVE chemical extinction equation (Pitchford et al., 2007) is:

$$\begin{aligned} b_{ext} \approx\ & 2.2 \times f_s(RH) \times [\text{Small Sulfate}] + 4.8 \times f_L(RH) \\ & \times [\text{Large Sulfate}] + 2.4 \times f_s(RH) \times [\text{Small Nitrate}] + 5.1 \\ & \times f_L(RH) \times [\text{Large Nitrate}] + 2.8 \times [\text{Small Organic Mass}] \\ & + 6.1 \times [\text{Large Organic Mass}] + 10 \times [\text{Elemental Carbon}] \\ & + 1 \times [\text{Soil dust}] + 1.7 \times f_{ss}(RH) \times [\text{Sea Salt}] + 0.6 \\ & \times [\text{Coarse Mass}] + \text{Rayleigh Scattering(Site Specific)} + 0.33 \\ & \times [NO_2](ppb) \end{aligned} \quad (6)$$

The Large and Small sulfate indicate formation through dry and aqueous mechanisms (John et al., 1990) and are defined by the IMPROVE equation as:

$$[\text{Large Sulfate}] = [\text{Total Sulfate}]^2/20, \text{for}[\text{Total Sulfate}] < 20\ \mu g\ m^{-3} \quad (7)$$

$$[\text{Large Sulfate}] = [\text{Total Sulfate}], \text{for}[\text{Total Sulfate}] \geq 20\ \mu g\ m^{-3} \quad (8)$$

$$[\text{Small Sulfate}] = [\text{Total Sulfate}] - [\text{Large Sulfate}] \quad (9)$$

The same method is used to separate total nitrate and organic mass (OM) concentrations into the Large and Small size fractions. OM was estimated by multiplying the OC by 1.6, which is suitable for urban aerosol (Turpin and Lim, 2001; Cao et al., 2005). The soil fraction was estimated from the Fe level according to the global crustal abundance of 3.5% (Taylor and McLenna, 1985):

$$\text{Soil dust} = (1/0.035) \times [Fe] = 28.57 \times [Fe] \quad (10)$$

The positive matrix factorization (PMF) solution to the Chemical Mass Balance (CMB) receptor model (Paatero and Tapper, 1994; Watson et al., 2008) was used to assess potential sources of visibility degradation. The PMF model was run multiple times, extracting three to six factors. Each run was initialized with random starting points, and the most physically interpretable profiles were found with a four factor solution. The frequency distribution of scaled residuals was taken into account, most of which were between −2 and +2, ensuring a good agreement between the PMF model results and the input data. As with most PMF–CMB solutions, there are indications of some mixing of sources within each factor (Watson and Chow, 2012). Linear regression analysis was used to estimate source contribution to $b_{sp,dry}$. The regression coefficients were then multiplied by the normalized source contributions to calculate the contribution of each source factor to the respective aerosol property for each sample.

4. Results and discussion

4.1. Seasonal variations of visibility

Daily averaged VR (Supplemental Fig. S1) varied from 0.6 to 28.5 km, with an average of 6.4 ± 4.5 km. Table 1 shows that average VR was 35–45% higher in spring (8.0 km) and summer (7.4 km) than during autumn (4.8 km) and winter (4.5 km). Although average VR in 2009 was ~23% higher than 2007 (Chang et al., 2009), it was lower than those reported from other large Chinese cities such as Beijing, Tianjin, Nanjing, Guangzhou, and Shanghai (Chang et al., 2009; Deng et al., 2011; Zhao et al., 2011).

As shown in Supplemental Fig. S2, wind speeds (1.8 m s^{-1}) and temperature (20.0 °C) during spring and summer indicate greater vertical mixing and horizontal dispersion than during winter, resulting in lower $PM_{2.5}$ mass. Higher precipitation during spring and summer (465.4 mm or 70.4% of the 2009 precipitation; China Statistical Yearbook, 2010) could also scavenge pollutants. Average $PM_{2.5}$ concentrations during autumn and winter were 171.4 and 203.4 μg m^{-3}, respectively, 1.2–2.0 times higher than during the other seasons. Reduced visibility during autumn and winter was associated with higher secondary inorganic aerosols and organic carbon, with RH in the range of 67–78%. This differs from Beijing, where the lowest VR is found in summer and also associated with high RH (Zhang et al., 2010).

PM_{10} concentrations were translated to an air pollution index (API; see Table S1) in the "Blue Sky Project" (Zhang et al., 2010). Air quality is considered good when PM_{10} is below 150 μg m^3 with API < 100. This criterion resulted in 304 "Blue Sky" days during

Table 1
Seasonal averages of light extinction and visual range (VR) in Xi'an from mid-February to December 2009.

Parameter[a]	$b_{sp,dry}$ (Mm^{-1})[b]	$b_{sp,wet}$ (Mm^{-1})[c]	b_{ap} (Mm^{-1})[d]	b_{ag} (Mm^{-1})[e]	b_{sg} (Mm^{-1})[f]	b_{ext} (Mm^{-1})[g]	VR (km)[h]
Spring	434.3 ± 247.0	632.2 ± 488.7	72.7 ± 34.7	8.0 ± 2.5	10	711 ± 499	8.0 ± 4.9
% of b_{ext}	67.7	83.9	12.6	1.5	2.0		
Summer	454.5 ± 267.4	798.0 ± 694.4	57.5 ± 21.2	6.3 ± 2.2	10	867 ± 697	7.4 ± 4.3
% of b_{ext}	62.1	86.4	10.5	1.2	1.9		
Autumn	606.3 ± 310.4	1307.1 ± 1080.4	106.7 ± 55.4	8.6 ± 2.2	10	1434 ± 1114	4.8 ± 3.6
% of b_{ext}	46.8	88.3	9.6	0.9	1.2		
Winter	657.4 ± 436.9	1488.0 ± 1332.2	104.0 ± 69.6	8.3 ± 2.8	10	1607 ± 1361	4.5 ± 3.7
% of b_{ext}	52.8	86.8	10.9	1.1	1.2		
Annual	525.3 ± 338.7	1009.2 ± 994.6	82.6 ± 52.3	7.7 ± 2.6	10	1102 ± 1020	6.4 ± 4.5
% of b_{ext}	58.2	86.3	10.9	1.2	1.6		

[a] The four seasons were designated as December and mid-February for winter, March to May for spring, June–August for summer, and September– November for autumn.
[b] Dry scattering coefficient measured by nephelometer at RH < 60%.
[c] Wet scattering coefficient modified by ambient RH.
[d] Absorption by aerosols calculated from 10 (m^2 g^{-1}) × [EC](μg m^{-3}).
[e] Absorption by gas calculated from 0.33 × [NO_2] (ppb).
[f] Rayleigh scattering.
[g] Light extinction estimated by sum of daily $b_{sp,wet}$, b_{ap}, b_{ag}, and b_{sg}, then averaged over each season.
[h] Visual range (VR) calculated from 3.912/b_{ext} × 1000 km.

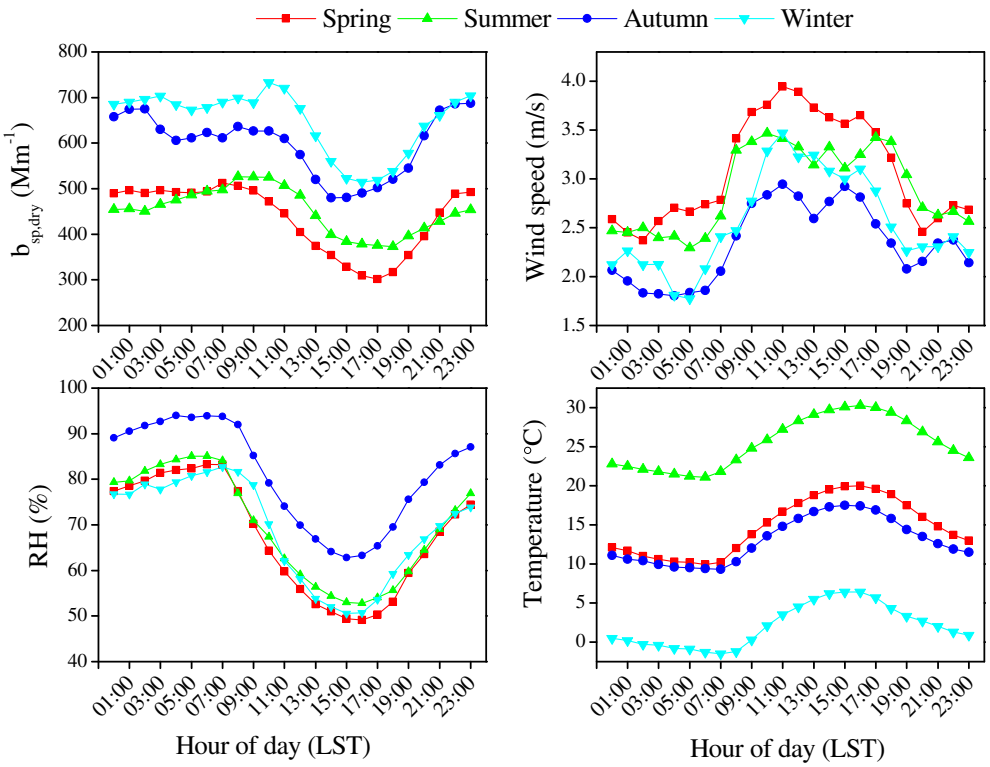

Fig. 1. Diurnal variations of hourly averaged dry light scattering coefficient ($b_{sp,dry}$), wind speed, relative humidity (RH), and temperature changes during spring (March to May), summer (June to August), autumn (September to November), and winter (December to mid-February) in 2009.

2009 (China Statistical Yearbook, 2010), ~80% of which occurred during the study period (see Supplemental Fig. S1). Optical measurements from this study, however, show ~65% of "Blue Sky" days were hazy (VR < 10 km and RH < 80%, China Meteorological Administration, 2010).

As shown in Table 1, the wet light scattering coefficient ($b_{sp,wet}$) had the highest contribution to b_{ext}, in the range of 632–1488 Mm^{-1}, accounting for ~84–88% of b_{ext}. Light scattering by dry particles ($b_{sp,dry}$) was correlated with $PM_{2.5}$ mass ($r = 0.7$), and ranged from 434 to 657 Mm^{-1}, accounting for 83–87% of dry b_{ext}. Similar single scattering albedos (i.e. $w_0 = b_{sp}/b_{ext}$) were also found in the Pearl River and Yangtze River Delta regions of China (Cheng et al., 2008; Deng et al., 2008; Xu et al., 2002). The particle absorption coefficient (b_{ap}) contributed to 10–13% of b_{ext}, with the remaining 2–4% attributed to gases.

Fig. 1 presents the diurnal variations of $b_{sp,dry}$ and meteorological conditions. It shows elevated morning (0800–1000 LST) and evening (2300 LST) $b_{sp,dry}$ with minimum during afternoon (1400–1700 LST). Evening highs and afternoon lows in $b_{sp,dry}$ corresponded to the diurnal RH measurements. Elevated RH at night enhances the growth of hygroscopic particles (i.e. sulfates and nitrates) to sizes that scatter more light. These diurnal variations are similar to those found in other urban areas (Lyamani et al., 2008; Pereira et al., 2011); mainly driven by variations of emission sources and meteorological conditions (Pereira et al., 2008). Morning peaks in $b_{sp,dry}$ coincide with lower dispersion (i.e., low wind speed) and high emissions from traffic during rush hours (Cao et al., 2009). The decrease after the morning peak is associated with coupling of the surface inversion layer to layers aloft, low RH, and high wind speeds. The increase in $b_{sp,dry}$ during the evening hours

Table 2
Correlation among $PM_{2.5}$ mass, chemical components, meteorological observables, and visual range (VR) during 2009 ($r > 0.8$ are shown in bold).

	VR	$PM_{2.5}$	SO_4^{2-}	NO_3^-	Cl^-	NH_4^+	K^+	Mg^{2+}	Ca^{2+}	OC	EC	NO_2	RH	WS
VR	1.00													
$PM_{2.5}$	−0.57	1.00												
SO_4^{2-}	−0.63	**0.81**	1.00											
NO_3^-	−0.62	**0.82**	**0.80**	1.00										
Cl^-	−0.39	0.77	0.54	0.61	1.00									
NH_4^+	−0.71	**0.83**	**0.96**	**0.90**	0.58	1.00								
K^+	−0.50	**0.88**	0.78	**0.83**	0.78	**0.80**	1.00							
Mg^{2+}	−0.01	0.03	0.13	−0.06	0.13	0.08	0.02	1.00						
Ca^{2+}	0.03	0.18	−0.07	0.12	0.19	−0.07	0.19	0.25	1.00					
OC	−0.37	**0.82**	0.60	0.71	**0.83**	0.65	**0.86**	0.00	0.20	1.00				
EC	−0.44	**0.83**	0.66	0.76	0.79	0.69	**0.86**	−0.07	0.17	**0.87**	1.00			
NO_2	−0.33	0.68	0.52	0.64	0.55	0.54	0.70	−0.08	0.20	0.66	0.74	1.00		
RH	−0.71	0.24	0.49	0.46	0.19	0.57	0.26	0.12	−0.16	0.16	0.18	0.01	1.00	
WS	0.30	−0.31	−0.27	−0.31	−0.33	−0.29	−0.35	−0.10	−0.05	−0.42	−0.45	−0.44	−0.17	1.00

r: correlation coefficient; VR: visual range; OC: organic carbon; EC: elemental carbon; RH: relative humidity; WS: wind speed.

is attributed to the evening rush hour, increased domestic cooking and heating emissions, and formation of the nighttime surface inversion.

4.2. Correlation of visual range with $PM_{2.5}$ and meteorological parameters

The correlation matrix in Table 2 illustrates that VR was negatively correlated with RH ($r = -0.71$), $PM_{2.5}$ ($r = -0.57$), and NO_2 ($r = -0.33$). This is consistent with Fig. 2, which shows that most of the days with low VR (<5 km) were associated with high RH (~90%) without precipitation.

VRs in Fig. 2 are exponentially associated with $PM_{2.5}$ mass, consistent with the linear relationship between $PM_{2.5}$ and b_{ext}. The threshold $PM_{2.5}$ mass corresponding to VR <10 km was ~88 μg m^{-3}. This value was ~17% higher than the 75 μg m^{-3} adopted by the China Meteorological Administration (2010) to define hazy days, but was much lower than VR <10 km $PM_{2.5}$ mass value for Beijing (~110 μg m^{-3}) (Zhao et al., 2011). VR was not correlated with wind speed ($r = 0.30$). However, ~90% of days with VR <10 km were associated with wind speeds <1.0 m s^{-1} and no precipitation (RH < 80%).

VR was negatively related to secondary inorganic ions (SO_4^{2-}, NO_3^-, and NH_4^+) with correlations in the range of −0.71 to −0.62, consistent with previous studies (Tao et al., 2009; Yang et al., 2007; Yuan et al., 2006). High correlations ($0.81 < r < 0.88$) were found between $PM_{2.5}$ mass and major constituents: anions (SO_4^{2-} and NO_3^-), cation (NH_4^+), and carbon (OC and EC). Water-soluble potassium (K^+) was correlated with $PM_{2.5}$ mass ($r = 0.88$), carbon (OC and EC, $r = 0.86$), and Cl^- ($r = 0.78$), consistent with biomass burning contributions.

4.3. Effect of $PM_{2.5}$ chemical composition on light extinction

Chemical b_{ext} (based on the revised IMPROVE equation), was highest during winter (1328 Mm^{-1}), followed by autumn (1316 Mm^{-1}), spring (659 Mm^{-1}), and summer (602 Mm^{-1}), with an annual average of 912 ± 882 Mm^{-1}. Average chemical b_{ext} in Xi'an was 1.3–3.1 times higher than that measured in Jinan, China (292 Mm^{-1}, Yang et al., 2007), Guangzhou, China (367 Mm^{-1}, Jung et al., 2009), and Seoul, Korea (704 Mm^{-1}, Kim et al., 2006). As shown in Fig. 3, $(NH_4)_2SO_4$ was the largest contributor accounting for 39.8% of b_{ext}, consistent with previous studies (Tao et al., 2009; Yang et al., 2007). OM (23.8%) and NH_4NO_3 (23.1%) contributions were also important. Higher NH_4NO_3 contributions were apparent during autumn, while OM contributions were important for all seasons (Fig. 3). Particle light absorption (b_{ap}) from EC contributed 9.1% of b_{ext}.

For non-urban IMPROVE sites, Malm and Day (2000) found sulfates contributed ~60–70% of b_{ext} in the eastern United States, while OM contributed ~35% of b_{ext} in the western United States. Chan et al. (1999) found that poor visibility in Brisbane, Australia was associated with traffic emissions, followed by secondary

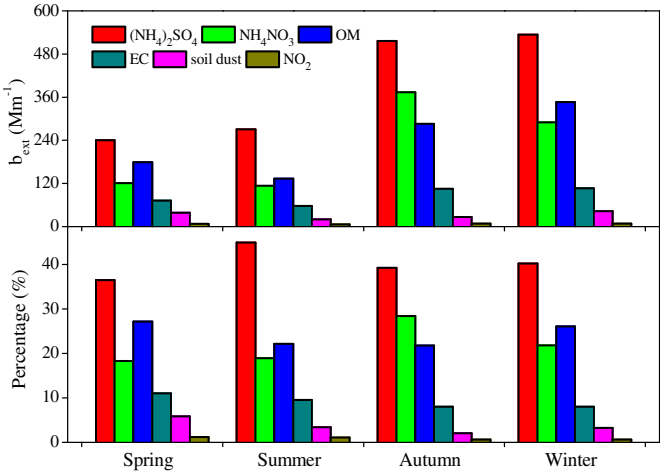

Fig. 3. Relative contributions of $PM_{2.5}$ chemical components to light extinction coefficient (b_{ext}) based on the revised IMPROVE equation: $b_{ext} \approx 2.2 \times f_s(RH) \times$ [Small Sulfate] + 4.8 × $f_L(RH)$ × [Large Sulfate] + 2.4 × $f_s(RH)$ × [Small Nitrate] + 5.1 × $f_L(RH)$ × [Large Nitrate] + 2.8 × [Small Organic Mass] + 6.1 × [Large Organic Mass] + 10 × [Elemental Carbon] + 1 × [Soil dust] + 1.7 × $f_{ss}(RH)$ × [Sea Salt] + 0.6 × [Coarse Mass] + Rayleigh Scattering (Site Specific) + 0.33 × [NO_2] (ppb). Organic Mass = 1.6 × OC.

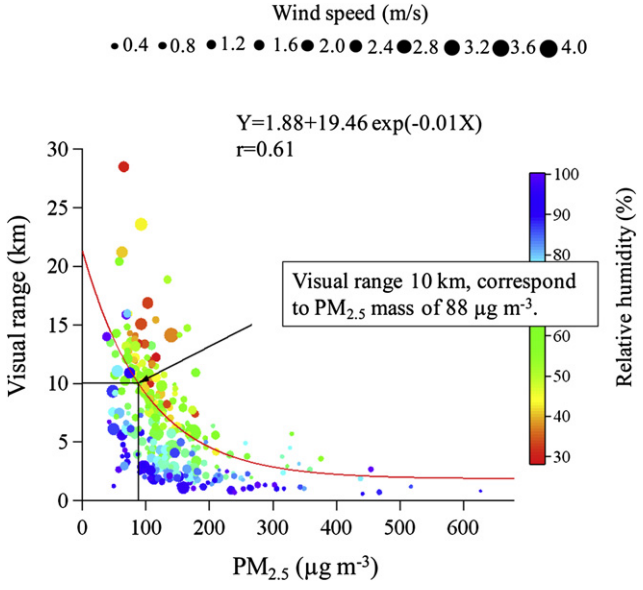

Fig. 2. Visual range as a function of $PM_{2.5}$ mass in Xi'an from February to December 2009. Data points are color coded for relative humidity and size coded for wind speed. The exponential fitted curve is based days with relative humidity <80% and visual range below 10 km.

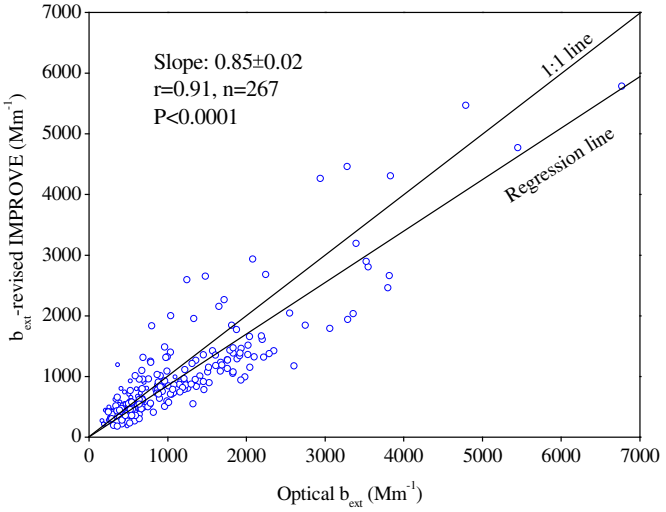

Fig. 4. Relationship of chemical b_{ext} based on the revised IMPROVE equation to measured b_{ext} (See footnote to Table 1 for sum of $b_{sp,wet}$, b_{ap}, b_{ag}, and b_{sg} for b_{ext} calculation).

Table 3
Contributions of major $PM_{2.5}$ chemical components and NO_2 to light extinction during Type I (visual range (VR) > 10 km), Type II (5 < VR ≤ 10 km), Type III (1 < VR ≤ 5 km), and Type IV (VR ≤ 1 km) (unit in Mm^{-1}) conditions.

Parameter	Type I b_{ext}		Type II b_{ext}		Type III b_{ext}		Type IV b_{ext}	
	Average	S.D.	Average	S.D.	Average	S.D.	Average	S.D.
$(NH_4)_2SO_4$	115.2	103.9	187.5	103.9	607.8	412.1	2663.5	311.5
NH_4NO_3	32.1	28.9	92.5	68.2	379.4	256.8	1490.1	334.3
OM	146.5	68.4	180.3	86.2	266.8	204.8	866.1	379.9
EC	49.2	16.5	73.7	34.5	101.9	59.6	246.4	29.5
Soil dust	31.6	24.8	33.1	29.6	25.4	18.1	62.2	4.9
NO_2	6.3	1.6	7.2	2.4	8.7	2.7	13.7	1.1

b_{ext}: Light extinction coefficient; OM: Organic mass = 1.6 × OC; EC: Elemental carbon. Soil dust: Estimated by Fe/0.035; and S.D.: Standard deviation.

sulfates and biomass burning. For urban sites, Yang et al. (2007) and Jung et al. (2009) found that $(NH_4)_2SO_4$ was the largest contributor (41%–47%) to b_{ext} in Jinan and Guangzhou, followed by OM (~22%).

According to the Xi'an Statistical Yearbook (2010), coal burning (a major source of energy generation) was over 7.85×10^6 tons in 2009, with ~93% used to generate electricity and heating. Annual SO_2 emissions were estimated to be 8.3×10^4 tons. More coal combustion in the winter heating season (middle of November to the following middle of March) is consistent with elevated light scattering by $(NH_4)_2SO_4$ (534 Mm^{-1}), and lower VR.

Chemical b_{ext} slightly underestimated optical b_{ext} as shown in Fig. 4, with a regression slope of 0.85 ± 0.02 and $r = 0.91$. The revised IMPROVE equation (see Eq. (6)) is a reasonable starting point for b_{ext} in Xi'an, but more locally-derived dry scattering and absorption coefficients and f(RH) might improve the agreement. These would require more specific measurements of particle size as a function of RH (Pitchford and McMurry, 1994).

VR is sorted into four categories in Table 3 to compare variations in chemical components under good to poor visibility: Type I (VR > 10 km), Type II (5 < VR ≤ 10 km), Type III (1 < VR ≤ 5 km), and Type IV (VR ≤ 1 km). For Type I, OM (38.5%) was the largest b_{ext} contributor, followed by $(NH_4)_2SO_4$ (30.2%) and NH_4NO_3 (8.4%). For Type IV, $(NH_4)_2SO_4$ (49.9%) and NH_4NO_3 (27.9%) accounted for nearly 80% of b_{ext}, similar to Type III, with >70% of b_{ext} from $(NH_4)_2SO_4$ and NH_4NO_3. Although OM increased with lower VR, its relative contributions varied from 16.2 to 31.4% of b_{ext}.

Table 4 shows increases in most of the chemical species concentrations (except for Ca^{2+} and Mg^{2+}) corresponding with lower VR. For Types III and IV visibility conditions, SO_4^{2-} and NO_3^- concentrations were 2.9–9.2 and 5.1–14.1 times higher than for Type I good visibility, respectively.

Table 4
Average chemical component concentrations and meteorological parameters during Type I (visual range (VR) > 10 km), Type II (5 < VR ≤ 10 km), Type III (1 < VR ≤ 5 km), and Type IV (VR ≤ 1 km) conditions.

Observable[a]	Type I		Type II		Type III		Type IV	
	Average	S.D.[b]	Average	S.D.	Average	S.D.	Average	S.D.
$PM_{2.5}$	96.0	51.1	118.2	43.9	183.4	85.9	511.8	100.6
SO_4^{2-}	12.0	8.4	16.0	6.8	35.2	17.5	109.9	8.6
NO_3^-	4.4	2.3	9.1	5.3	22.3	13.1	62.0	2.2
Cl^-	3.4	3.6	3.7	2.3	5.8	5.4	14.7	3.5
NH_4^+	1.6	1.4	4.1	2.7	12.6	6.3	36.1	1.4
K^+	0.7	0.4	1.1	0.6	2.0	1.7	6.4	1.3
Mg^{2+}	0.5	1.3	0.3	0.3	0.3	0.4	0.3	0.2
Ca^{2+}	1.9	2.1	1.7	1.6	1.5	1.3	1.1	0.6
OM	24.3	10.8	29.9	13.7	42.1	26.6	142.0	62.3
EC	4.9	1.6	7.4	3.5	10.2	6.0	24.6	2.9
RH	51.7	16	61.9	14.3	80.7	11.3	90.0	2.6
WS	1.9	0.5	1.7	0.7	1.4	0.6	0.8	0.4

[a] Units: $PM_{2.5}$ and chemical species, μg m^{-3}, Relative humidity (RH), %; Wind speed (WS), m s^{-1}.
[b] S.D.: Standard deviation.

4.4. Source apportionment of visibility degradation

The PMF–CMB used $PM_{2.5}$ OC, EC, Ca, Mg, S, K, Ti, Mn, Fe, As, Br, and Pb to apportion $b_{sp,dry}$ to source factors. Derived source factors and contribution estimates are shown in Supplemental Fig. S3 and Fig. 5, respectively. The largest source factor, contributing 52.2% to $b_{sp,dry}$, was loaded on S, As, and Pb and was assigned to coal combustion. This factor contributed 60.7% in winter, 53.6% in autumn, 47.2% in spring, and 45.2% in summer, consistent with variations for $PM_{2.5}$ mass and energy consumption (Cao et al., 2009).

Factor 2 was enriched in EC, Br, and Pb, and was assigned to engine exhaust (Xu et al., 2012), accounting for 30.8% of $b_{sp,dry}$, with the highest during summer (39.3%). The total number of motor vehicles in Xi'an increased from $\sim 5.4 \times 10^5$ in 2005 to $\sim 10.1 \times 10^5$ in 2009 (Xi'an Statistical Yearbook, 2010). Engine NO_x emissions are related to NO_3^- levels. Gasoline and diesel engine exhaust contain light-absorbing EC, indicative of incomplete combustion (Cao et al., 2006; Watson et al., 1994).

Factor 3 had high loadings on K and OC, and was assigned to biomass burning (Duan et al., 2004; Xie et al., 2008). In nearby non-urban areas, wheat straw and maize stalks are burned for cooking year round, and burned for heating during winter. This source accounted for 12.3% of $b_{sp,dry}$.

Factor 4 had high loadings on Ca, Mg, Ti, Fe, and Mn, and was assigned to fugitive dust (Cao et al., 2008; Xie et al., 2008). An estimated ~283 km^2 (~27% of total area of Xi'an) was under construction during the study period (Xi'an Statistical Yearbook, 2010). Construction dust as well as vehicle-related resuspended road dust contributed 4.7% of $b_{sp,dry}$, with the highest during spring

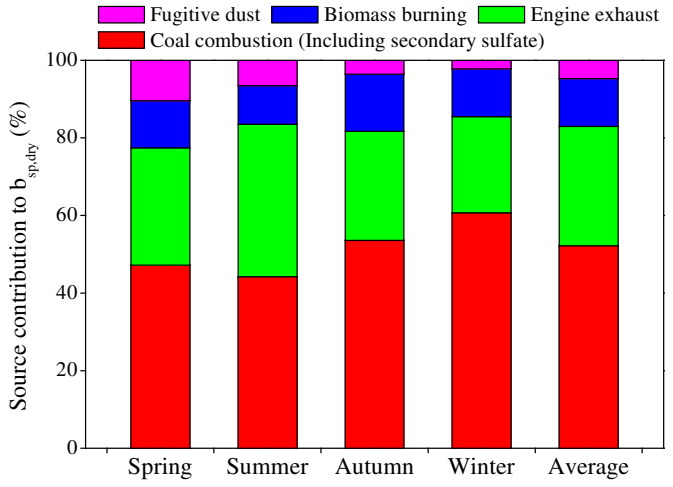

Fig. 5. Average source contribution (in percent) of each PMF–CMB source factor to dry particle light scattering coefficient ($b_{sp,dry}$) for each season from February 15 to December 31, 2009 in Xi'an, China.

(10.4%) when wind speed was faster than other seasons (see Supplemental Fig. S2).

5. Conclusions

Daily dry particle light scattering coefficients, $PM_{2.5}$, NO_2 were collected in Xi'an from February 15 to December 31, 2009 to investigate the causes of visibility degradation and its temporal variability. Average VR was 6.4 ± 4.5 km, with the largest seasonal variations found in spring (1.5–28.5 km), followed by summer (1.2–18.9 km). The lowest VR was found in winter (0.8–10.7 km), mainly due to the elevated $PM_{2.5}$ mass, sulfates, and nitrates. Diurnal particle light scattering coefficients ($b_{sp,dry}$) showed early morning and late evening peaks with a low in the afternoon hours. This diurnal cycle was likely due to variations of emission sources and meteorological conditions. Elevated $PM_{2.5}$ mass was associated with VR <10 km, and a $PM_{2.5}$ threshold value of 88 μg m^{-3} (i.e., low visibility occurs when $PM_{2.5} > 88$ μg m^{-3}).

Based on the revised IMPROVE equation, $(NH_4)_2SO_4$ was the largest contributor, accounting for 39.8% of light extinction coefficient, followed by OM (23.8%), NH_4NO_3 (23.1%), and EC (9.1%), with minor contribution from soil dust (3.4%) and NO_2 (0.8%). Chemical extinction was ~15% lower than optical extinction, but they were highly correlated. Elevated concentrations of secondary aerosol species (i.e. SO_4^{2-} and NO_3^-) were the main causes of VR <5 km.

The PMF solution to the CMB receptor model indicated that coal combustion (52.2%) was the largest contributor to $b_{sp,dry}$, followed by engine exhaust (30.8%), biomass burning (12.3%), and fugitive dust (4.7%). Approximately 65% of "Blue Sky" days reported by the provincial government corresponded to VR <10 km.

Acknowledgments

This work was supported by the Natural Science Foundation of China (NSFC40925009), the Chinese Academy of Sciences (Project Numbers O929011018, KZCX2-YW-BR-10, KZCX2-YW-148) and the Ministry of Science & Technology (2009IM030100). The National Center for Atmospheric Research is sponsored by the National Science Foundation. The authors also thank Dr. Antony Chen from Desert Research Institute for PMF technical comments and suggestions.

Appendix A. Supplementary material

Supplementary data related to this article can be found online at http://dx.doi.org/10.1016/j.atmosenv.2012.05.036.

References

Booker, R.L., Douglas, C.A., 1977. Visual Range Concepts, Instrumental Determination and Aviation Application. Report Number NBS-159; prepared by U.S. Department of Commerce, Washington DC.

Cao, J.J., Lee, S.C., Ho, K.F., Zhang, X.Y., Zou, S.C., Fung, K., Chow, J.C., Watson, J.G., 2003. Characteristics of carbonaceous aerosol in Pearl River Delta Region, China during 2001 winter period. Atmospheric Environment 37, 1451–1460.

Cao, J.J., Wu, F., Chow, J.C., Lee, S.C., Li, Y., Chen, S.W., An, Z.S., Fung, K.K., Watson, J.G., Zhu, C.S., Liu, S.X., 2005. Characterization and source apportionment of atmospheric organic and elemental carbon during fall and winter of 2003 in Xi'an, China. Atmospheric Chemistry and Physics 5, 3127–3137.

Cao, J.J., Lee, S.C., Ho, K.F., Fung, K., Chow, J.C., Watson, J.G., 2006. Characterization of roadside fine particulate carbon and its eight fractions in Hong Kong. Aerosol and Air Quality Research 6, 106–122.

Cao, J.J., Chow, J.C., Watson, J.G., Wu, F., Han, Y.M., Jin, Z.D., Shen, Z.X., An, Z.S., 2008. Size-differentiated source profiles for fugitive dust in the Chinese Loess Plateau. Atmospheric Environment 42, 2261–2275.

Cao, J.J., Zhu, C.S., Chow, J.C., Watson, J.G., Han, Y.M., Wang, G.H., Shen, Z.X., An, Z.S., 2009. Black carbon relationships with emissions and meteorology in Xi'an, China. Atmospheric Research 94, 194–202.

Chan, Y., Simpson, R., McTainsh, G.H., Vowles, P.D., Cohen, D., Bailey, G., 1999. Source apportionment of visibility degradation problems in Brisbane (Australia) using the multiple linear regression techniques. Atmospheric Environment 33, 3237–3250.

Chang, D., Song, Y., Liu, B., 2009. Visibility trends in six megacities in China 1973–2007. Atmospheric Research 94, 161–167.

Che, H., Zhang, X., Li, Y., Zhou, Z., Qu, J.J., Hao, X., 2009. Haze trends over the capital cities of 31 provinces in China, 1981–2005. Theoretical and Applied Climatology 97, 235–242.

Cheng, Y.F., Wiedensohler, A., Eichler, H., Su, H., Gnauk, T., Brüggemann, E., Herrmann, H., Heintzenberg, J., Slanina, J., Tuch, T., Hu, M., Zhang, Y.H., 2008. Aerosol optical properties and related chemical apportionment at Xinken in Pearl River Delta of China. Atmospheric Environment 42, 6351–6372.

China Meteorological Administration, 2010. Observation and Forecasting Levels of Haze. QX/T 113–2010 (in Chinese).

China Statistical Yearbook, 2010, http://www.stats.gov.cn/tjsj/ndsj/2010/indexch.htm.

Chow, J.C., Watson, J.G., 1999. Ion chromatography in elemental analysis of airborne particles. In: Landsberger, S., Creatchman, M. (Eds.), 1999. Elemental Analysis of Airborne Particles, vol. 1. Gordon and Breach Science, Amsterdam, pp. 97–137.

Chow, J.C., Watson, J.G., 2011. Air quality management of multiple pollutants and multiple effects. Air Quality and Climate Change Journal 45, 26–32.

Chow, J.C., Watson, J.G., Pritchett, L.C., Pierson, W.R., Frazier, C.A., Purcell, R.G., 1993. The DRI thermal/optical reflectance carbon analysis system: description, evaluation and applications in U.S. Air quality studies. Atmospheric Environment. Part A. General Topics 27, 1185–1201.

Chow, J.C., Watson, J.G., Crow, D., Lowenthal, D.H., Merrifield, T., 2001. Comparison of IMPROVE and NIOSH carbon measurements. Aerosol Science and Technology 34, 23–34.

Chow, J.C., Bachmann, J.D., Wierman, S.S.G., Mathai, C.V., Malm, W.C., White, W.H., Mueller, P.K., Kumar, N., Watson, J.G., 2002a. Critical review discussion–visibility: science and regulation. Journal of the Air & Waste Management Association 52, 973–999.

Chow, J.C., Engelbrecht, J.P., Watson, J.G., Wilson, W.E., Frank, N.H., Zhu, T., 2002b. Designing monitoring networks to represent outdoor human exposure. Chemosphere 49, 961–978.

Chow, J.C., Watson, J.G., Chen, L.W.A., Arnott, W.P., Moosmuller, H., 2004. Equivalence of elemental carbon by thermal/optical reflectance and transmittance with different temperature protocols. Environmental Science & Technology 38, 4414–4422.

Chow, J.C., Watson, J.G., Chen, L.W.A., Paredes-Miranda, G., Chang, M.C.O., Trimble, D., Fung, K.K., Zhang, H., Zhen Yu, J., 2005. Refining temperature measures in thermal/optical carbon analysis. Atmospheric Chemistry and Physics 5, 2961–2972.

Chow, J.C., Watson, J.G., Chen, L.W.A., Chang, M.C.O., Robinson, N.F., Trimble, D., Kohl, S., 2007. The IMPROVE-A temperature protocol for thermal/optical carbon analysis: maintaining consistency with a long-term database. Journal of the Air & Waste Management Association 57, 1014–1023.

Chow, J.C., Watson, J.G., Chen, L.W.A., Rice, J., Frank, N.H., 2010a. Quantification of $PM_{2.5}$ organic carbon sampling artifacts in US networks. Atmospheric Chemistry and Physics 10, 5223–5239.

Chow, J.C., Watson, J.G., Green, M.C., Frank, N.H., 2010b. Filter light attenuation as a surrogate for elemental carbon. Journal of the Air & Waste Management Association 60, 1365–1375.

Chow, J.C., Watson, J.G., Robles, J., Wang, X., Chen, L.W.A., Trimble, D.L., Kohl, S.D., Tropp, R.J., Fung, K.K., 2011. Quality assurance and quality control for thermal/optical analysis of aerosol samples for organic and elemental carbon. Analytical and Bioanalytical Chemistry 401, 3141–3152.

Deng, X.J., Tie, X.X., Wu, D., Zhou, X.J., Bi, X.Y., Tan, H.B., Li, F., Jiang, C.L., 2008. Long-term trend of visibility and its characterizations in the Pearl River Delta (PRD) region, China. Atmospheric Environment 42, 1424–1435.

Deng, J., Wang, T., Jiang, Z., Xie, M., Zhang, R., Huang, X., Zhu, J., 2011. Characterization of visibility and its affecting factors over Nanjing, China. Atmospheric Research 101, 681–691.

Duan, F., Liu, X., Yu, T., Cachier, H., 2004. Identification and estimate of biomass burning contribution to the urban aerosol organic carbon concentrations in Beijing. Atmospheric Environment 38, 1275–1282.

Han, Y.M., Cao, J.J., Lee, S.C., Ho, K.F., An, Z.S., 2010. Different characteristics of char and soot in the atmosphere and their ratio as an indicator for source identification in Xi'an, China. Atmospheric Chemistry and Physics 10, 595–607.

Hodkinson, J.R., 1966. Calculations of colour and visibility in urban atmospheres polluted by gaseous NO_2. Air and Water Pollution 10, 137–144.

John, W., Wall, S.M., Ondo, J.L., Winklmayr, W., 1990. Modes in the size distributions of atmospheric inorganic aerosol. Atmospheric Environment. Part A. General Topics 24, 2349–2359.

Jung, J., Lee, H., Kim, Y.J., Liu, X., Zhang, Y., Gu, J., Fan, S., 2009. Aerosol chemistry and the effect of aerosol water content on visibility impairment and radiative forcing in Guangzhou during the 2006 Pearl River Delta campaign. Journal of Environmental Management 90, 3231–3244.

Kim, Y.J., Kim, K.W., Kim, S.D., Lee, B.K., Han, J.S., 2006. Fine particulate matter characteristics and its impact on visibility impairment at two urban sites in Korea: Seoul and Incheon. Atmospheric Environment 40, 593–605.

Koschmieder, H., 1924a. Theorie der horizontalen Sichtweite. Beiträge zur Physik der freien Atmosphäre 12, 33–53.

Koschmieder, H., 1924b. Theorie der horizontalen sichtweite II. Kontrast und Sichtweite (Theory of horizontal visibility). Meteorologische Zeitschrift 12, 171–181.

Lyamani, H., Olmo, F.J., Alados-Arboledas, L., 2008. Light scattering and absorption properties of aerosol particles in the urban environment of Granada, Spain. Atmospheric Environment 42, 2630–2642.

Malm, W.C., Day, D.E., 2000. Optical properties of aerosols at Grand Canyon national park. Atmospheric Environment 34, 3373–3391.

Malm, W.C., Day, D.E., Kreidenweis, S.M., Collett, J.L., Lee, T., 2003. Humidity-dependent optical properties of fine particles during the Big Bend regional aerosol and visibility observational study. Journal of Geophysical Research 108 (D9), 4279. http://dx.doi.org/10.1029/2002JD002998.

Paatero, P., Tapper, U., 1994. Positive matrix factorization: a non-negative factor model with optimal utilization of error estimates of data values. Environmetrics 5, 111–126.

Pereira, S., Wagner, F., Silva, A.M., 2008. Scattering properties and mass concentration of local and long-range transported aerosols over the South Western Iberia Peninsula. Atmospheric Environment 42, 7623–7631.

Pereira, S.N., Wagner, F., Silva, A.M., 2011. Seven years of measurements of aerosol scattering properties, near the surface, in the southwestern Iberia Peninsula. Atmospheric Chemistry and Physics 11, 17–29.

Pitchford, M.L., McMurry, P.H., 1994. Relationship between measured water vapor growth and chemistry of atmospheric aerosol for Grand Canyon, Arizona, in winter 1990. Atmospheric Environment 28, 827–839.

Pitchford, M., Malm, W., Schichtel, B., Kumar, N., Lowenthal, D., Hand, J., 2007. Revised algorithm for estimating light extinction from IMPROVE particle speciation data. Journal of the Air & Waste Management Association 57, 1326–1336.

Shen, Z.X., Cao, J.J., Arimoto, R., Han, Z.W., Zhang, R.J., Han, Y.M., Liu, S.X., Okuda, T., Nakao, S., Tanaka, S., 2009. Ionic composition of TSP and $PM_{2.5}$ during dust storms and air pollution episodes at Xi'an, China. Atmospheric Environment 43, 2911–2918.

Tao, J., Ho, K.F., Chen, L., Zhu, L., Han, J., Xu, Z., 2009. Effect of chemical composition of $PM_{2.5}$ on visibility in Guangzhou, China, 2007 spring. Particuology 7, 68–75.

Taylor, S.R., McLenna, S.M., 1985. The Continental Crust: Its Composition and Evolution. Blackwell, Oxford. 315 p.

Turpin, B.J., Lim, H.J., 2001. Species contributions to $PM_{2.5}$ mass concentrations: revisiting common assumptions for estimating organic mass. Aerosol Science and Technology 35, 602–610.

Watson, J.G., Chow, J.C, 2012. Source apportionment. In: El-Shaarwi, A.H., Piegorsch, W.W. (Eds.), The Encyclopedia of Environmetrics. John Wiley & Sons, Ltd.:, Hoboken, NJ.

Watson, J.G., Chow, J.C., Fujita, E.M., Lu, Z., Heisler, S.L., Moore, T.A., 1994. Wintertime Source Contributions to Light Extinction in Tucson. AZ. 26 September 94 A.D. Snowbird, UT, 1187 p.

Watson, J.G., Chow, J.C., Frazier, C.A., 1999. X-ray fluorescence analysis of ambient air samples. Elemental Analysis of Particles 1, 67–96.

Watson, J.G., Chen, L.-W.A., Chow, J.C., Lowenthal, D.H., Doraiswamy, P., 2008. Source apportionment: findings from the U.S. Supersite Program. Journal of the Air & Waste Management Association 58, 265–288.

Watson, J.G., Chow, J.C., Chen, L.W.A., Frank, N.H., 2009. Methods to assess carbonaceous aerosol sampling artifacts for IMPROVE and other long-term networks. Journal of the Air & Waste Management Association 59, 898–911.

Watson, J.G., 2002. Visibility: science and regulation. Journal of the Air & Waste Management Association 52, 628–713.

Xi'an Municipal Bureau of Statistics and NBS Survey Office in Xi'an, 2010. Xi'an Statistical Yearbook. China Statistics Press, pp. 208–210 (in Chinese).

Xie, S.D., Liu, Z., Chen, T., Hua, L., 2008. Spatiotemporal variations of ambient PM_{10} source contributions in Beijing in 2004 using positive matrix factorization. Atmospheric Chemistry and Physics 8, 2710–2716.

Xu, J., Bergin, M.H., Yu, X., Liu, G., Zhao, J., Carrico, C.M., Baumann, K., 2002. Measurement of aerosol chemical, physical and radiative properties in the Yangtze delta region of China. Atmospheric Environment 36, 161–173.

Xu, H.M., Cao, J.J., Ho, K.F., Ding, H., Han, Y.M., Wang, G.H., Chow, J.C., Watson, J.G., Khol, S.D., Qiang, J., Li, W.T., 2012. Lead concentrations in fine particulate matter after the phasing out of leaded gasoline in Xi'an, China. Atmospheric Environment 46, 217–224.

Yang, L.X., Wang, D.C., Cheng, S.H., Wang, Z., Zhou, Y., Zhou, X.H., Wang, W.X., 2007. Influence of meteorological conditions and particulate matter on visual range impairment in Jinan, China. Science of the Total Environment 383, 164–173.

Yuan, C.-S., Lee, C.-G., Liu, S.-H., Chang, J.-C., Yuan, C., Yang, H.-Y., 2006. Correlation of atmospheric visibility with chemical composition of Kaohsiung aerosols. Atmospheric Research 82, 663–679.

Zhang, Q., Zhang, J., Xue, H., 2010. The challenge of improving visibility in Beijing. Atmospheric Chemistry and Physics 10, 7821–7827.

Zhao, P., Zhang, X., Xu, X., Zhao, X., 2011. Long-term visibility trends and characteristics in the region of Beijing, Tianjin, and Hebei, China. Atmospheric Research 101, 711–718.